ELSEVIER

Contents lists available at ScienceDirect

Chemical Physics Impact

journal homepage: www.sciencedirect.com/journal/chemical-physics-impact





Hydrothermally synthesized rGO-BiVO₄ nanocomposites for photocatalytic degradation of RhB

N. Kannan ^a, P. Sundara Venkatesh ^{a, *}, M. Ganesh Babu ^a, G. Paulraj ^{b, c}, K. Jeganathan ^b

- ^a Nanomaterials Laboratory, Department of Physics, Sri S. Ramasamy Naidu Memorial College (Affiliated to Madurai Kamaraj University, Madurai 625 021, Tamil Nadu, India), Sattur 626203, Tamil Nadu, India
- ^b Centre for Nanoscience and Nanotechnology, Department of Physics, Bharathidasan University, Tiruchirappalli 620024, Tamil Nadu, India
- ^c Photonics Laboratory, Computer, Electrical, and Mathematical Science and Engineering Division, King Abdullah University of Science and Technology, Thuwal 23955-6900. Kingdom of Saudi Arabia

ARTICLE INFO

Keywords: rGO BiVO₄ Hybrid Nanocomposites Dye degradation

ABSTRACT

BiVO₄ nanoparticles (NPs) synthesized by hydrothermal approach were hybridized with reduced graphene oxide (rGO) in various weight ratios (1:1, 1:3 & 3:1) and their effect of the composition on improving the photocatalytic degradation performance of the RhB dye was evaluated. The size and morphological variation of BiVO₄ due to the hybridization of rGO have been analyzed with scanning electron microscopy and X-Ray diffraction studies, which confirms the formation of the composition. The intimate contact between 2D graphene oxide and BiVO₄ is expected to lend higher separation of charge carriers due to the built-in electric field at the interface. A reduction in the bandgap of BiVO₄ from 2.4 to 2.1 eV was demonstrated by UV-DRS and can be associated with the correct addition of rGO in BiVO₄ NPs. In addition, Raman spectroscopy confirms the chemical reduction of GO in the hybrid nanocomposites. The photocatalytic analysis shows that 3:1-rGO-BiVO₄ (3:1-RGB) nanocomposites have an almost 3.6 times higher performance in the complete degradation of RhB dyes as compared to bare BiVO₄ NPs.

1. Introduction

In the last few decades, the pollution of natural resources has increased enormously due to enormous industrialization and rapid population growth. Human health is strongly linked to our environment. Hence, many efforts have been made to control environmental pollution. For this reason, much attention is paid to the treatment of industrial wastewater. In terms of a sustainable environment, approaches such as reverse osmosis, ion exchange, solvent extraction, and chlorination are the conventional way of extracting waste from water resources [1]. However, high cost and the least efficiency limit its practical use towards industrial viability. In this regard, there is an urgent need to develop a cost-effective and highly efficient garbage remover for treating complex sewage effluents. To achieve this goal, the photocatalytic removal of water contaminants is a fascinating and economically viable approach to address the above problem [2]. In particular, the photocatalytic degradation of dye molecules depends on the properties of the catalytic materials such as size, light absorption capacity, and chemical stability [3]. Usually, nanomaterials are excellent photocatalysts due to their increased surface area and the simple bandgap technique [4]. Narrow bandgap materials with rich catalytic centers are ideal catalyst choices to achieve excellent performance with maximum efficiency since visible light covers the maximum part of the solar spectrum [5] and visible light can be utilized with the help of the notable narrow bandgap semiconductors such as $BiVO_4$, α - Fe_2O_3 , WO_3 , and MoS_2 .

Among these narrow bandgap semiconductors, the monoclinic phase-gated bismuth vanadium oxide (BiVO₄) is one of the best photocatalysts in visible light [6] owing to its non-corrosive, narrow bandgap (2.4 eV) and biocompatible nature. As a result, BiVO₄ is extensively investigated for photocatalytic dye degradation, photo-electrocatalytic hydrogen generation, photovoltaic applications, electrochemical sensors, etc. [7–11]. On the other hand, the high rate of photo-induced charge recombination strongly influences the independent BiVO₄ for commercial applications [12]. This can be overcome by approaches such as doping with metal ions, heterojunction formation, and composite formation. For this reason, the production of nanocomposites with carbon-containing materials is attracting great interest due to their ease of processing, and cost-effectiveness [13–15].

E-mail address: srnmcphysics@gmail.com (P.S. Venkatesh).

^{*} Corresponding author.

From this perspective, graphene is the shining star of the carbon family and offers excellent electronic conductivity, high inherent strength, very good flexibility, high thermal conductivity, and a large surface area [16–18]. The versatility of graphene lends itself very well to supercapacitor electrodes, sensors, and photocatalytic materials [19, 20]. However, the exfoliation of graphene is extremely difficult because it requires complicated instruments and time-consuming processes. This can be addressed by graphene oxide (GO), as it can be easily and inexpensively synthesized on a large scale with uncompromising physical and chemical properties [21].

It has been shown that the hybridization of rGO with transition metal oxides could create an excellent platform for electron transfer that facilitates fine-tuning of the photocatalytic performance. In this study, BiVO₄ NPs and rGO-BiVO₄ nanocomposites with different weight ratios (1:3, 1:1 & 3:1) were synthesized by the *in-situ* hydrothermal method. The 3:1-rGO-BiVO₄ nanocomposites show excellent photocatalytic performance against 20 ppm RhB within 120 min.

2. Experimental details

2.1. Preparation of GO

Modified Hummer's method was adopted for the synthesis of GO. In a typical procedure, 4 g of graphite powder and 2 g of sodium nitrate (NaNO₃) were dissolved with 200 ml of Conc. Sulfuric Acid (H₂SO₄) under magnetic stirring. This solution was maintained at 20 °C by immersing in an ice bath. After an hour, 12 g of potassium permanganate (KMnO₄) was gradually added, and the temperature of the solution was carefully maintained below 10 °C for 1 hour. This is followed by vigorous stirring of the mixture at 35 °C for almost 18 h. Then, 1000 ml of water was added to the above solution, and its temperature rapidly raised to 98 °C with effervescence. At last, the mixture turned from dark brown to brownish-yellow with the successful addition of 10 ml of 50 wt % $\rm H_2O_2$. Finally, the prepared solution was washed with diluted HCl and double distilled (DD) water several times to remove the unwanted metal ions present in the prepared solution. Finally, it is dried under a vacuum.

2.2. Synthesis of rGO-BiVO₄ nanocomposites

To prepare BiVO₄, 1.99 g of Bi(NO₃) $_3$ ·SH $_2$ O and 0.935 g of NH $_4$ VO $_3$ were mixed with 40 ml of 1 M HNO $_3$ solution and stirred for 1 hour. In the meantime, 1 M NaOH solution was dropped and wisely added to the above mixture until 6 pH was achieved. Then, the resultant yellow-colored solution was transferred to a Teflon-lined autoclave and treated hydrothermally at 120 °C for 4 h and the solution was allowed to cool naturally. The obtained product was centrifuged and washed with DD water, and ethanol 3 times to remove the unreacted residues. Finally, the collected semisolid sample was subjected to vacuum drying to get BiVO $_4$ NPs and calcinated at 400 °C for 60 min [22].

To synthesize rGO-BiVO₄ nanocomposites, 100 mg/40 ml of GO and 100 mg/40 ml of BiVO₄ were taken separately and sonicated for 1 hour. After the completion of sonication, both solutions were mixed and mildly stirred for 30 min. 1 ml of hydrazine hydrate (35%) was added successively, to the dispersed solution to reduce GO. After that, the prepared solution was transferred to a Teflon-lined autoclave for thermal treatment at 120 °C for 2 h. The obtained product was centrifuged and dried. The final product was labeled as 1:1-RGB (1:1-rGO-BiVO₄). The same protocol is followed to prepare other compositions of rGO-BiVO₄ nanocomposites [1:3-rGO-BiVO₄ (named as 1:3-RGB) & 3:1-rGO-BiVO₄ (named as 3:1-RGB)].

2.3. Evaluation of photocatalytic activities against RHB

The photocatalytic dye removal efficiency of BiVO₄ and rGO-BiVO₄ nanocomposites was tested against 20 mg $\rm L^{-1}$ (20 ppm) RhB dye. The suspension of 20 mg of BiVO₄ and each nanocomposite in 50 ml of 20

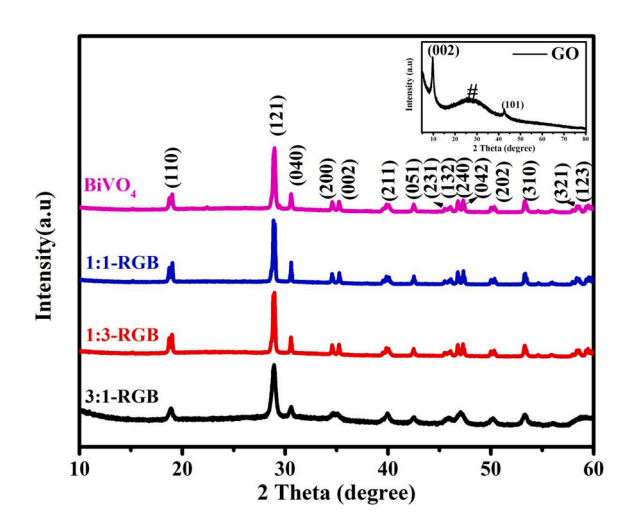


Fig. 1. XRD patterns of $BiVO_4$ and different compositions of $rGO\text{-}BiVO_4$ nanocomposites with GO in the inset.

ppm RhB solution was sonicated in the dark (30 min) in order to produce an adsorption-desorption equilibrium. The photocatalytic activity was examined under direct sunlight. All of this work was done on a sunny day in Sattur, Tamil Nadu, India (geographical location 9.37 N 77.93E) from 11 a.m. to 2 p.m. In the specified time interval, 3 ml aliquots were taken at regular intervals of 15 min from 0 to 120 min. UV–Vis absorption spectra were recorded with a UV–Vis spectrophotometer for the filtered solutions. The RhB dye degradation efficiency of the prepared photocatalyst was determined by suppressing the absorption peak at 554 nm.

2.3.1. Radical trapping experiment

In order to investigate the role of reactive species in the photocatalytic degradation process, a radical trapping experiment was carried out against the highly efficient photocatalyst among the synthesized nanocomposites (here 3:1-RGB). In the present analysis, 1 mM benzo-quinone (BQ), isopropyl alcohol, and ethylene diamine tetra acetic acid (EDTA) were used as superoxide quenchers (O_2), hydroxyl quenchers (OH) and hole quenchers (h^+) and dissolved in the RhB dye solution in addition to the superior photocatalyst.

2.4. Material characterizations

The structural analysis was carried out using an X-ray diffractometer (Bruker D8 Advance, Germany) with Cu K_α radiation of wavelength $\lambda{=}1.5406$ Å. The morphological analyses have been performed by a field emission scanning electron microscope (FESEM, Carl Zeiss-Sigma, Germany). The reflectance spectra of the samples were explored using a UV–visible spectrophotometer (JASCO V-750, Japan). Raman spectroscopy analysis has been studied with the help of Raman microscopic systems (NT-MDT, Russia) with a 473 nm laser (spot size ${\sim}0.5~\mu m$ in diameter Cobalt laser).

3. Results and discussion

The typical X-ray diffraction patterns of BiVO₄ NPs and rGO-BiVO₄ nanocomposites are shown in Fig. 1. All peaks of BiVO₄—NPs matched perfectly with the monoclinic phase of BiVO₄ (JCPDS Card No.: 014–688) and the absence of impurity peaks clearly shows the high purity of the sample. The main peaks developed in the GO are indicated in the inset of Fig. 1 and agree well with previous reports [23,24]. The peak broadening and the lower intensity of this peak mean the good formation of GO and the peak at 26.480 $^{\circ}$ (#) centered corresponds to the reflection plane (002) of graphite [25]. In the XRD spectra of the composites, the absence of GO peaks facilitates the deepening of the BiVO₄

Table 1
Measured lattice parameters, crystalline size, and unit cell volume of BiVO₄NPs and rGO-BiVO₄ nanocomposites .

Sample	a (Å)	b (Å)	c (Å)	β (degree)	d ₁₂₁ (Å)	FWHM of (121) Plane	Crystalline Size, D (nm)	Unit Cell Volume (Å) ³
BiVO ₄	5.176	11.695	5.085	89.894	3.085	0.245	34.97	307.835
1:1-RGB	5.178	11.694	5.083	89.946	3.084	0.244	35.17	307.769
1:3-RGB	5.178	11.700	5.087	89.951	3.085	0.244	35.28	308.242
3:1-RGB	5.194	11.682	5.073	91.434	3.086	0.415	20.65	307.686

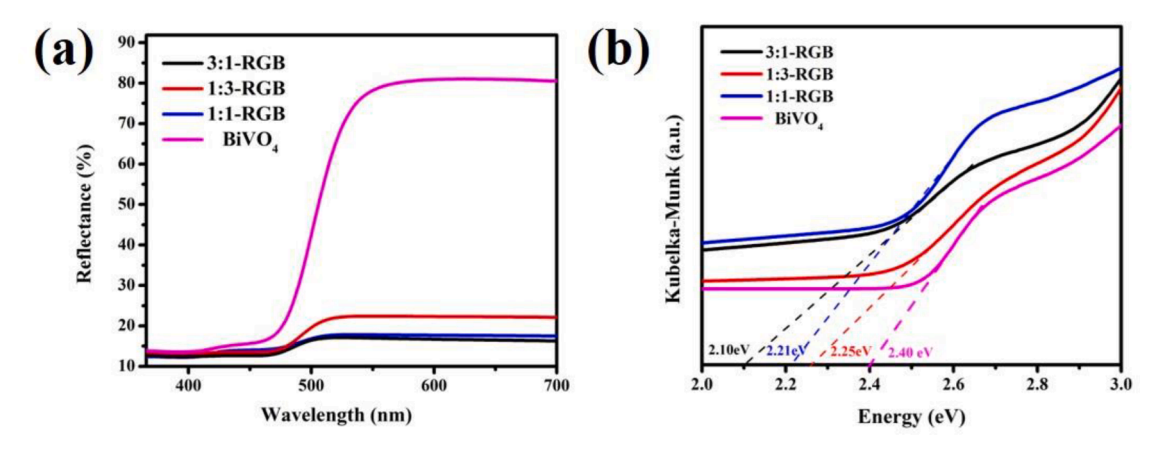


Fig. 2. (a) UV-Vis diffuse reflectance spectra and (b) estimated bandgap values of BiVO₄ NPs and rGO-BiVO₄ nanocomposites from Kubelka-Munk function.

NPs in the graphene matrix and the relatively lower intensity of the GO peaks than that of $BiVO_4$. In order to observe the structural difference in the synthesized $BiVO_4$ -rGO, lattice parameters, crystallite size, and unit cell volume were examined. The values are calculated using the relations (1) (2) & (3) and are shown in Table 1.

$$\frac{1}{d^2} = \frac{1}{\sin^2 \beta} \left(\frac{h^2}{a^2} + \frac{k^2 \sin^2 \beta}{b^2} + \frac{l^2}{c^2} - \frac{2hl \cos \beta}{ac} \right) \tag{1}$$

$$D = \frac{0.94 \times \lambda}{\beta \cos \theta} \tag{2}$$

$$V = abc \sin\beta \tag{3}$$

It should be noted that the crystallite size of the BiVO₄ NPs (34.97 nm) was significantly reduced by the large addition of GO [i.e., the size of 3:1 RGB is 20.65 nm]. This size reduction is possibly due to the presence of functional groups in the GO. Similarly, the crystal size increased slightly with the high loading of BiVO₄ in the composition (i. e., 1: 3 RGB) compared to that of pure BiVO₄ NPs.

In order to gain insights into the optical properties of the synthesized BiVO₄ and rGO-BiVO₄ nanocomposites, UV–Vis reflection spectra were recorded, which show that the reflection of BiVO₄ decreases drastically about the loading volume of rGO as shown in Fig. 2. This significant feature is caused by the color changes stimulated by the improved composition of GO. The optical bandgap was calculated from the K-M plot by using the following relation (4). The calibrated bandgap values are in the order of BiVO₄> 1:3-RGB > 1:1- RGB > 3:1-RGB and their numerical values are given in Table 3. It corroborates with earlier reports [26].

$$F(R) = \frac{(1-R)^2}{2R} \tag{4}$$

Further, for the higher concentrations of the rGO-BiVO $_4$ composites (4:1-RGB and 5:1 RGB), the bandgap lies in the infrared range as shown in the supporting information (Fig. S1). Consequently, the photocatalytic dye degradation performance of these composites is negligible as compared to their counterparts. From the observation, it is noticed that the excessive loading of rGO forms an adhesion layer on the surface

of BiVO₄ and consequently reduces the degradation efficiency of those samples.

The surface morphology of the synthesized GO, BiVO₄, and several ratios of the rGO-BiVO₄ nanocomposites are summarized in Fig. 3. From Fig. 3 (a) and (b), it can be seen that the chemically synthesized GO is present in a layer structure with a layer thickness of ~ 7 nm and also shows the presence of a large surface. Strongly nucleated, non-uniform rod-shaped nanostructures were found in BiVO₄ (Fig. 3 (c)), and the graphene layer is well connected to BiVO₄ NPs in the 1:1 RGB nanocomposites (Fig. 3 (d)). This interesting feature specifies the strong bond between BiVO₄ and rGO and in particular the length and diameter of the BiVO₄ nanostructures, which are limited by the large composition of GO in the 3:1-RGB nanocomposites (Fig. 3 (f)) as compared to an equal ratio of 1:1-RGB nanocomposites (Fig. 3 (d)). The average values of the length and the diameter of the bare BiVO₄ and the various weight ratios of the rGO-BiVO₄ sample are tabulated (Table 2). The tabular results were consistent with the XRD results.

Raman spectroscopy is the best-known approach to characterize carbonaceous materials. Fig. 4 shows the recorded Raman spectra of GO, BiVO₄, and rGO-BiVO₄ nanocomposites. Two dominant peaks appear at 1339 and 1595 cm⁻¹, which are associated with the D and G modes, indicating structural defects or vibrations in the plane of C sp² atoms. A very broad peak centered at 776 cm⁻¹ (*) is related to the in-plane C—C-C ring, and less intense peaks at 2634 cm⁻¹ are assigned to the 2D mode of GO [27]. Raman spectra of rGO-BiVO₄ nanocomposites show the characteristic peaks at 817, and 702 cm⁻¹ (symmetrical stretching and asymmetrical modes of the V-O bond), 352, and 322 cm⁻¹ (symmetrical and anti-symmetrical bending modes of the VO₄ tetrahedra) and are connected with BiVO₄ [28]. It is clear that the intensity of the D, G bands and ν_s (V-O) varies with the variations of the GO and BiVO₄ compositions, and the decreased intensity of the 2D band in composites means the decrease in graphene layers and the formation of rGO [29].

The photocatalytic efficiency of the $BiVO_4$ NPs and $rGO-BiVO_4$ nanocomposites was investigated from the degradation studies of RhB under direct sunlight. The characteristic absorption peak of RhB is observed at 554 nm and its intensity is canceled according to the solar irradiation time, as shown in Fig. 5. It can be seen from the observations that the rate of degradation of RhB for $BiVO_4$ and $rGO-BiVO_4$

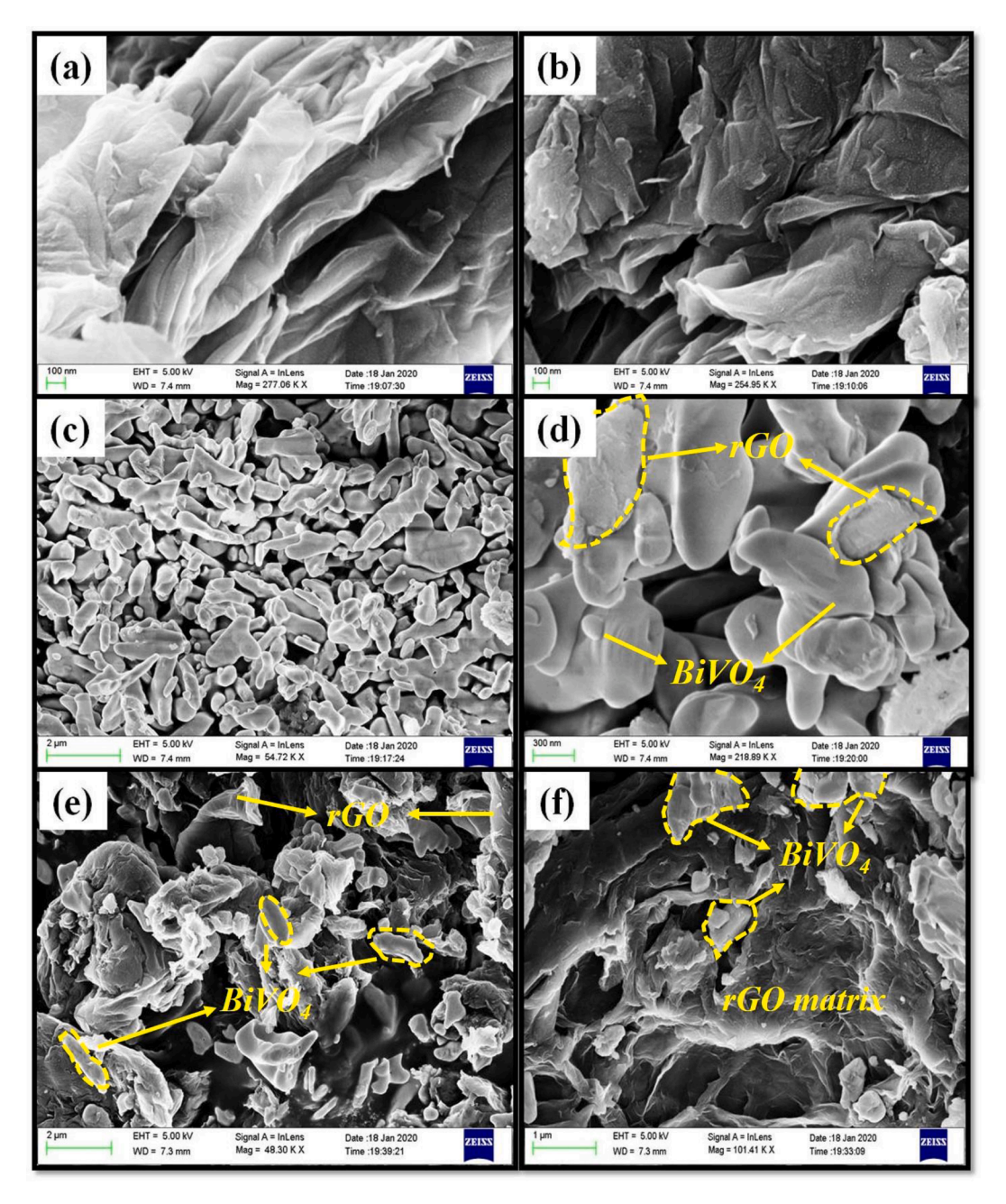


Fig. 3. FESEM images of (a-b) GO; (c) BiVO₄; (d) 1:1-RGB; (e) 1:3-RGB; (f) 3:1-RGB.

 $\label{eq:table 2} \textbf{Measured length and diameter of BiVO}_4 \ nanorods \ in \ the \ bare \ sample \ and \ its \ rGO \ composites.}$

Sample	Average Length (μm)	Average Diameter (nm)
BiVO ₄	1.05	334
1:1-RGB	1.09	352
1:3-RGB	1.20	436
3:1-RGB	0.55	262

nanocomposites varies as shown in Fig. 5 (a-d). In addition, Fig. 5 (e) shows the ln (Ct / C0) -time curve of the photodegradation of RhB by tested samples under irradiation with sunlight. Remarkably, the linear photocatalytic degradation of this organic dye molecule can be related to the pseudo-first-order reaction kinetics. The percentage of degradation was calculated using the relation (5) and $C_t\ \&\ C_0$ is the concentration at time t and initial concentration of RhB respectively.

$$Degradation Percentage = \left[1 - \frac{C_t}{C_0}\right] \times 100 \tag{5}$$

The absorption spectra show a percentage degradation of only 23.39% for the BiVO₄ catalyst after 120 min of solar irradiation. This low percentage of degradation can be attributed to the rapid recombination rate of electrons and holes that are generated in the semiconducting photocatalyst [30]. On the other hand, different volumes of rGO-loaded BiVO₄ NPs show an excellent degradation performance with a degradation percentage of 36.58, 75.15 and 92.51% for 1:3-RGB, 1:1-RGB, and 3:1-RGB nanocomposites respectively. This improved photocatalytic activity is due to the bandgap tuning and the increased surface area with the strong binding of BiVO₄ to the graphene matrix. In addition, the rGO reduces the rapid recombination of charge carriers by trapping the electrons and shifts the electron-hole recombination directly down. In order to obtain a constant of the degradation rate (K), a

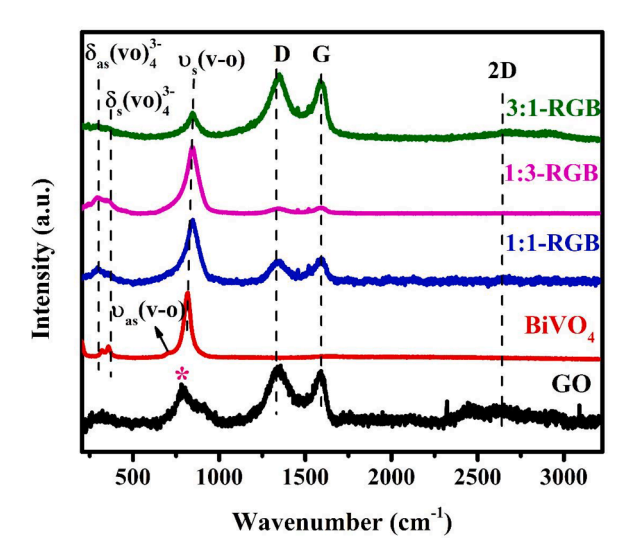


Fig. 4. Raman spectra of GO, BiVO₄, and rGO-BiVO₄ nanocomposites (1:1-RGB, 1:3-RGB and 3:1-RGB).

kinetic fit plot was created between ln (Ct / C0) and the reaction time (Fig. 5 (e)). The calculated K values for BiVO₄, 1:1-RGB, 1:3-RGB, and 3:1-RGB are listed in Table 3.

The degradation of RhB dye by 3:1 RGB possibly occurs by the following way. When the sunlight falls on the surface of BiVO₄, the separation of charge carriers will take place, where the electrons are excited into the conduction band (CB) by leaving the holes in the valence band (VB). The photoexcited electrons in the CB of BiVO₄ are easily transferred to the CB of rGO. Due to the conjugated Π - Π system, the rGO better mobility was attained for the photogenerated electrons which avoid the recombination of photo-separated electrons and holes. These electrons and holes in the composite sample (3:1-RGB) react with O₂ and H₂O offer superoxide ('O₂) and hydroxyl ('OH') radicals. The generated free radicals and remaining electrons in CB potentially degrade the RhB dye into CO₂ and H₂O.

In order to investigate the role of reactive species in the photocatalytic degradation process, a radical trapping experiment was carried out against the highly efficient photocatalyst among the synthesized nanocomposites (3:1-RGB). In the present analysis, 1 mM benzoquinone (BQ), isopropyl alcohol and ethylene diamine tetra acetic acid (EDTA) were used as superoxide quenchers ($^{\circ}$ C₂), hydroxyl quenchers ($^{\circ}$ OH) and hole quenchers ($^{\circ}$ H) respectively and dissolved in the RhB dye solution in addition to the superior photocatalyst. The results obtained from the radical trapping experiment are provided as a bar diagram in Fig. 5 (f). The scavenger analysis notifies that the addition of EDTA (hole quencher) predominantly suppresses the photodegradation efficiency. Following that BQ (superoxide quencher) also shows comparable suppression of RhB degradation. From the radical trapping analysis, it is noticed that $^{+}$ and $^{\circ}$ C₂ are the major contributors to the photocatalytic degradation of RhB dye by using a 3:1-RGB composite.

The excellent photocatalytic RhB degradation performance of 3:1 RGB is compared with recently published nanocomposites and shown in Table 4 and it shows the quality of the synthesized 3:1 RGB nanocomposite for photocatalytic degradation. Interestingly, 20 mg 3:1-RGB shows an excellent degradation against RhB with high concentration and minimal time interval under freely available sunlight. This confirms that the 3:1 rGO-BiVO₄ is the more efficient and economically profitable photocatalyst against very hard dyes such as RhB.

4. Conclusion

A rod-shaped crystalline $BiVO_4$ NPs and nanocomposites with different weight ratios of rGO-BiVO_4 nanocomposites were successfully synthesized by a simple hydrothermal method. The XRD patterns of rGO-BiVO_4 nanocomposites show the broadening of the dominant peak due to mass amplification of GO and reduction in crystal size. The fine adhesion of $BiVO_4$ to the graphene matrix and the variation of length and diameter can be also seen from FESEM images. The tuning of the bandgap energy from 2.4 to 2.10 eV by appropriately mixing GO was

Table 3 Bandgap energy and photocatalytic degradation constant (K) of hydrothermally synthesized $BiVO_4$ & rGO-BiVO₄ nanocomposites.

Photocatalyst name	Bandgap value (eV)	K (min ⁻¹)
BiVO ₄	2.40	2.3970 x 10 ⁻³
1:3-RGB	2.25	3.7960×10^{-3}
1:1-RGB	2.21	1.1604×10^{-2}
3:1-RGB	2.10	2.1606×10^{-2}

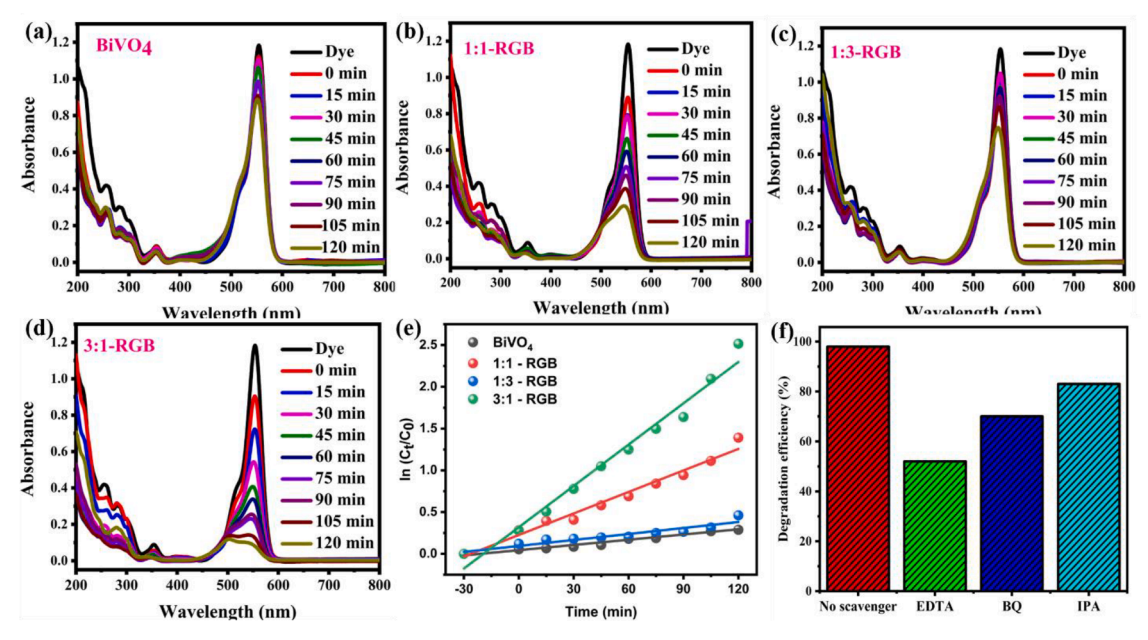


Fig. 5. Photocatalytic degradation of RhB over (a) BiVO₄ (b)1:1-RGB (c) 1:3-RGB (d) 3:1-RGB. (e) Degradation profile (f) Radical trapping results of 3:1 RGB.

Table 4Comparison of 3:1-RGB with previously reported nanocomposites.

Photocatalyst	Amount of catalyst	Concentration of RhB	Degradation period	Light source	Removal efficiency	Reference
CdSe/TiO ₂	50 mg	10 ppm	420 min	5 mW/cm ²	70%	[31]
Mn-doped CeO ₂	100 mg	10 ppm	210 min	300 W Hg arc lamp	65%	[32]
Bi ₂₅ FeO ₄₀ -rGO	40 mg	10 ppm	240 min	500 W Hg-Xe lamp	87%	[33]
rGO/ZnO-Bi ₂ MoO ₆	30 mg	10 ppm	150 min	400 W Mercury vapor lamp	79%	[34]
PANI-H ₂ SO ₄ -TKHP-50	10 mg	5 ppm	360 min	1500 W air-cooled Xenon lamp	78%	[35]
SrTiO ₃ /Bi ₅ O ₇ I	100 mg	20 ppm	150 min	500 W Xenon lamp	89.65%	[36]
3:1-RGB	20 mg	20 ppm	120 min	Direct sunlight	92.51%	Present work

confirmed from the UV-DRS spectra. Raman spectra provide evidence for the reduction of GO in the rGO-BiVO $_4$ nanocomposites. The 3:1 RGO-BiVO $_4$ shows 3.64 times better photocatalytic RhB degradation than the pure BiVO $_4$. The excellence in photocatalytic activity of 3:1 RGB nanocomposites was observed as compared to the previously reported nanocomposites.

CRediT authorship contribution statement

N. Kannan: Conceptualization, Methodology, Investigation, Visualization, Writing – original draft. P. Sundara Venkatesh: Conceptualization, Methodology, Investigation, Supervision, Writing – review & editing, Resources. M. Ganesh Babu: Conceptualization, Methodology, Investigation, Visualization, Writing – original draft. G. Paulraj: Resources, Writing – original draft. K. Jeganathan: Writing – review & editing, Resources.

Declaration of Competing Interest

The authors declare that they have no known competing financial interests or personal relationships that could have appeared to influence the work reported in this paper.

Data availability

Data will be made available on request.

Acknowledgment

PSV would like to express his sincere gratitude to the College Management and Principal for their generous financial support to develop a nanomaterials laboratory.

Supplementary materials

Supplementary material associated with this article can be found, in the online version, at doi:10.1016/j.chphi.2023.100230.

References

- J.P. Deebasree, V. Maheskumar, B. Vidhya, Investigation of the visible light photocatalytic activity of BiVO₄ prepared by sol-gel method assisted by ultrasonication, Ultrason. Sonochem. 45 (2018) 123–132, https://doi.org/ 10.1016/j.ultsonch.2018.02.002.
- [2] R. Ameta, S. Benjamin, A. Ameta, S.C. Ameta, Photocatalytic degradation of organic pollutants: a review, Mater. Sci. Forum. 734 (2013) 247–272, https://doi. org/10.4028/www.scientific.net/MSF.734.247.
- [3] N. Singh, J. Prakash, R.K. Gupta, Design and engineering of high-performance photocatalytic systems based on metal oxide-graphene-noble metal nanocomposites, Mol. Syst. Des. Eng. 2 (2017) 422–439, https://doi.org/10.1039/ c7me00038c.
- [4] W. Wang, G. Li, D. Xia, T. An, H. Zhao, P.K. Wong, Photocatalytic nanomaterials for solar-driven bacterial inactivation: recent progress and challenges, Environ. Sci. Nano. 4 (2017) 782–799, https://doi.org/10.1039/C7EN00063D.
- [5] D. Li, N. Ohashi, S. Hishita, T. Kolodiazİnnyi, H. Haneda, Origin of visible-light-driven photocatalysis: a comparative study on N/F-doped and N-F-codoped TiO2 powders by means of experimental characterizations and theoretical calculations,

- J. Solid State Chem. 178 (2005) 3293–3302, https://doi.org/10.1016/j.issc.2005.08.008.
- [6] J.K. Cooper, S. Gul, F.M. Toma, L. Chen, P.A. Glans, J. Guo, J.W. Ager, J. Yano, I. D. Sharp, Electronic structure of monoclinic BiVO4, Chem. Mater. 26 (2014) 5365–5373, https://doi.org/10.1021/cm5025074.
- [7] Y. Li, J. Zhu, H. Chu, J. Wei, F. Liu, M. Lv, J. Tang, B. Zhang, J. Yao, Z. Huo, L. Hu, S. Dai, BiVO4 semiconductor sensitized solar cells, Sci. China Chem. 58 (2015) 1489–1493, https://doi.org/10.1007/s11426-015-5348-3.
- [8] V.I. Merupo, S. Velumani, K. Ordon, N. Errien, J. Szade, A.H. Kassiba, Structural and optical characterization of ball-milled copper-doped bismuth vanadium oxide (BiVO4), CrystEngComm 17 (2015) 3366–3375, https://doi.org/10.1039/ c5ce00173k.
- [9] O. Monfort, L.C. Pop, S. Sfaelou, T. Plecenik, T. Roch, V. Dracopoulos, E. Stathatos, G. Plesch, P. Lianos, Photoelectrocatalytic hydrogen production by water splitting using BiVO4 photoanodes, Chem. Eng. J. 286 (2016) 91–97, https://doi.org/ 10.1016/j.cej.2015.10.043.
- [10] P. Gnanasekar, M. Kumar Eswaran, G. Palanichamy, T. Khee Ng, U. Schwingenschlögl, B.S. Ooi, J. Kulandaivel, Sustained Solar-Powered Electrocatalytic H2 Production by Seawater Splitting Using Two-Dimensional Vanadium Disulfide, ACS Sustain. Chem. Eng. 9 (2021) 8572–8580, https://doi. org/10.1021/acssuschemeng.1c01909.
- [11] G. Zafeiropoulos, P. Varadhan, H. Johnson, L. Kamphuis, A. Pandiyan, S. Kinge, M. C.M. van de Sanden, M.N. Tsampas, Rational design of photoelectrodes for the fully integrated polymer electrode membrane-photoelectrochemical water-splitting system: a case study of bismuth vanadate, ACS Appl. Energy Mater. 4 (2021) 9600–9610, https://doi.org/10.1021/acsaem.1c01752.
- [12] C. Zachäus, F.F. Abdi, L.M. Peter, R. Van De Krol, Photocurrent of BiVO4 is limited by surface recombination, not surface catalysis, Chem. Sci. 8 (2017) 3712–3719, https://doi.org/10.1039/c7sc00363c.
- [13] H.S. Park, K.E. Kweon, H. Ye, E. Paek, G.S. Hwang, A.J. Bard, Factors in the metal doping of BiVO4 for improved photoelectrocatalytic activity as studied by scanning electrochemical microscopy and first-principles density-functional calculation, J. Phys. Chem. C. 115 (2011) 17870–17879. https://doi.org/10.1021/bj0204492r.
- [14] S. Sun, W. Wang, Advanced chemical compositions and nanoarchitectures of bismuth based complex oxides for solar photocatalytic application, RSC Adv. 4 (2014) 47136–47152, https://doi.org/10.1039/c4ra06419d.
- [15] B. Jin, E. Jung, M. Ma, S. Kim, K. Zhang, J. Il Kim, Y. Son, J.H. Park, Solution-processed yolk-shell-shaped WO3/BiVO4 heterojunction photoelectrodes for efficient solar water splitting, J. Mater. Chem. A. 6 (2018) 2585–2592, https://doi.org/10.1039/c7ta08452h.
- [16] B.R. Smith, M.J. Conger, J.S. McMullen, M.J. Neubert, Why believe? The promise of research on the role of relgion in entrepreneurial action, J. Bus. Ventur. Insights. 11 (2019) e00119, https://doi.org/10.1016/j.jbvi.2019.e00119.
- [17] P. Dharmaraj, K. Jeganathan, V. Gokulakrishnan, P. Sundara Venkatesh, R. Parameshwari, V. Ramakrishnan, S. Balakumar, K. Asokan, K. Ramamurthi, Controlled and selective area growth of monolayer graphene on 4H-SiC substrate by electron-beam-assisted rapid heating, J. Phys. Chem. C. 117 (2013) 19195–19202, https://doi.org/10.1021/jp404483y.
- [18] P. Dharmaraj, P.S. Venkatesh, P. Kumar, K. Asokan, K. Jeganathan, Direct growth of few layer graphene on SiO 2 substrate by low energy carbon ion implantation, RSC Adv. (2016), https://doi.org/10.1039/C6RA20015J.
- [19] H. Huang, S. Su, N. Wu, H. Wan, S. Wan, H. Bi, L. Sun, Graphene-based sensors for human health monitoring, Front. Chem. 7 (2019) 1–26, https://doi.org/10.3389/ fchem.2019.00399.
- [20] X. Li, J. Cao, L. Yang, M. Wei, X. Liu, Q. Liu, Y. Hong, Y. Zhou, J. Yang, One-pot synthesis of ZnS nanowires/Cu 7 S 4 nanoparticles/reduced graphene oxide nanocomposites for supercapacitor and photocatalysis applications, Dalt. Trans. 48 (2019) 2442–2454, https://doi.org/10.1039/c8dt04097d.
- [21] V. Sharma, A. Garg, S.C. Sood, Graphene Synthesis via Exfoliation of Graphite by Ultrasonication, Int. J. Eng. Trends Technol. 26 (2015) 37–42, https://doi.org/ 10.14445/22315381/ijett-v26p208.
- [22] M. Ganeshbabu, N. Kannan, P.S. Venkatesh, G. Paulraj, K. Jeganathan, D. MubarakAli, Synthesis and characterization of BiVO4nanoparticles for environmental applications, RSC Adv. 10 (2020) 18315–18322, https://doi.org/ 10.1039/d0ra01065k.
- [23] F.T. Johra, J.W. Lee, W.G. Jung, Facile and safe graphene preparation on solution based platform, J. Ind. Eng. Chem. 20 (2014) 2883–2887, https://doi.org/ 10.1016/j.jiec.2013.11.022.
- [24] L. Stobinski, B. Lesiak, A. Malolepszy, M. Mazurkiewicz, B. Mierzwa, J. Zemek, P. Jiricek, I. Bieloshapka, Graphene oxide and reduced graphene oxide studied by the XRD, TEM and electron spectroscopy methods, J. Electron Spectros. Relat. Phenomena. 195 (2014) 145–154, https://doi.org/10.1016/j.elspec.2014.07.003.

- [25] X. Jiao, Y. Qiu, L. Zhang, X. Zhang, Comparison of the characteristic properties of reduced graphene oxides synthesized from natural graphites with different graphitization degrees, RSC Adv. 7 (2017) 52337–52344, https://doi.org/ 10.1039/c7ra10809e.
- [26] S. Phanichphant, A. Nakaruk, K. Chansaenpak, D. Channei, Evaluating the photocatalytic efficiency of the BiVO4/rGO photocatalyst, Sci. Rep. 9 (2019) 1–9, https://doi.org/10.1038/s41598-019-52589-5.
- [27] I. Childres, L.A. Jauregui, W. Park, H. Caoa, Y.P. Chena, Raman spectroscopy of graphene and related materials, New Dev. Phot. Mater. Res. (2013) 403–418.
- [28] V.I. Merupo, S. Velumani, Structural and Optical properties of Molybdenum doped Bismuth vanadate powders, 2 (2014) 0–4.
- [29] P.J. Sephra, P. Baraneedharan, M. Sivakumar, T.D. Thangadurai, K. Nehru, In situ growth of hexagonal-shaped α-Fe2O3 nanostructures over few layered graphene by hydrothermal method and their electrochemical performance, J. Mater. Sci. Mater. Electron. 29 (2018) 6898–6908, https://doi.org/10.1007/s10854-018-8676-1.
- [30] A. Malathi, J. Madhavan, M. Ashokkumar, P. Arunachalam, A review on BiVO4 photocatalyst: activity enhancement methods for solar photocatalytic applications, Appl. Catal. A Gen. 555 (2018) 47–74, https://doi.org/10.1016/J. APCATA.2018.02.010.
- [31] F. Laatar, H. Moussa, H. Alem, L. Balan, E. Girot, G. Medjahdi, H. Ezzaouia, R. Schneider, CdSe nanorod/TiO2 nanoparticle heterojunctions with enhanced

- solar- and visible-light photocatalytic activity, Beilstein J. Nanotechnol. 8 (2017) 2741–2752, https://doi.org/10.3762/bjnano.8.273.
- [32] P. Li, W. Zhang, X. Zhang, Z. Wang, X. Wang, S. Ran, Y. Lv, Synthesis, characterization, and photocatalytic properties of flower-like Mn-doped ceria, Mater. Res. 21 (2018) 2–7, https://doi.org/10.1590/1980-5373-mr-2018-0167.
- [33] M.A. Basith, R. Ahsan, I. Zarin, M.A. Jalil, Enhanced photocatalytic dye degradation and hydrogen production ability of Bi25FeO40-rGO nanocomposite and mechanism insight, Sci. Rep. 8 (2018) 33–35, https://doi.org/10.1038/ s41598-018-29402-w.
- [34] R. Hejazi, A.R. Mahjoub, A.H. Cheshme Khavar, Zeynab Khazaee, Novel visible-light-responsive rGO-ZnO@Bi2MOO6 nanocomposite with enhanced light harvesting and Z-scheme charge transfer for photodegradation and detoxification of RhB, Solid State Sci. 95 (2019), 105934, https://doi.org/10.1016/j.solidstatesciences.2019.105934.
- [35] R. Gottam, P. Srinivasan, D.D. La, S.V. Bhosale, Improving the photocatalytic activity of polyaniline and a porphyrin: via oxidation to obtain a salt and a chargetransfer complex, New J. Chem. 41 (2017) 14595–14601, https://doi.org/ 10.1039/c7nj02399e.
- [36] Y. Song, X. Hao, W. Dai, J. Zhao, Aqueous synthesis and photocatalytic performance of Bi 5 O 7 I microflowers, Nano 14 (2019), https://doi.org/10.1142/ \$1793292019500504.